Thin Solid Films 640 (2017) 45–51

Contents lists available at ScienceDirect

Thin Solid Films

journal homepage: www.elsevier.com/locate/tsf

Stress reduction mechanism of diamond-like carbon films incorporated with different Cu contents

Peng Guo [a,1], Xiaowei Li [a,b,1], Lili Sun [a], Rende Chen [a], Peiling Ke [a], Aiying Wang [a,*]

[a] Key Laboratory of Marine Materials and Related Technologies, Zhejiang Key Laboratory of Marine Materials and Protective Technologies, Ningbo Institute of Materials Technology and Engineering, Chinese Academy of Sciences, Ningbo 315201, PR China
[b] Center for Computational Science, Korea Institute of Science and Technology, Seoul 136-791, Republic of Korea

ARTICLE INFO

Article history:
Received 28 February 2017
Received in revised form 26 August 2017
Accepted 1 September 2017
Available online 04 September 2017

Keywords:
Diamond-like carbon
Cu incorporated
Stress reduction
Theoretical calculations

ABSTRACT

Cu incorporated diamond-like carbon (Cu-DLC) films were deposited on Si/glass substrate by a hybrid ion beam deposition system, which consists of a direct current (DC) magnetron sputtering of Cu target and a linear ion source. The Cu concentration (from 0.1 to 39.7 at.%) in the Cu-DLC films was controlled by varying the sputtering current. The dependence of residual stress, microstructure and atomic bond structure upon Cu concentration was investigated systematically. Results indicated that the nanoscale Cu particles began to evolve from the carbon matrix in the Cu concentration range of 2.6–7.0 at.%. The residual stress of the Cu-DLC films (less than 0.60 GPa) showed a significant reduction compared with that of the pure carbon film (2.0 GPa). Theoretical calculations revealed that the formation of antibonding between Cu and C and the relaxation of distorted bond angles and bond length accounted for the significant reduction of residual stress caused by Cu incorporation.

1. Introduction

Due to their excellent properties such as high hardness, low coefficient of friction, and good chemical inertness [1], diamond-like carbon (DLC) films have been widely used in the fields of car parts, hydrophobic surface, gas barrier and electronics devices [2–6]. However, high residual stress of DLC films is the major drawback for their wider practical application [7,8]. Recently, the addition of metal element (Mo, W, Cr, Ti, Al, Cu, Ag, Au, etc.) into DLC films has been adopted as an effective way to reduce stress [9–24]. In general, at lower doping concentration those incorporated metal atoms would be dissolved in the DLC matrix, but at higher doping concentration some carbide forming elements such as Mo, W, Cr and Ti would gather into nanoscale carbide particles, while others such as Al, Ag, Au and Cu atoms would be distributed as nanoscale metal particles in the DLC matrix. For example, using reactive magnetron sputtering, Corbella et al. [9] reported that W and Mo incorporated DLC showed nearly no stress when the relative methane flow ratios was 0.03, and they discovered that stress was proportional to lattice parameter variation from the unstrained state. Wang and coworkers [10,11] proposed that at the lower W doping level, part of the W atoms were distributed in the DLC matrix without bonding with carbon atoms, which provided the pivot location for the bond distortion and reduced the film compressive stress. Ji et al. [13] proposed that the interface and grain boundary effects due to nanoscale MoC particles in the DLC matrix would cause stress reduction. Chen et al. [20] found that nanoscale Cu particles in the DLC matrix could reduce the film stress to 0.7 GPa and improve the critical load to 80 N for sample with 11 at.% Cu, and they thought that the stress reduction could be explained from the change of sp^3 concentration due to incorporated Cu atoms.

Obviously, due to the limited experimental characterization, the stress reduction mechanism caused by metal element incorporation is still unclear and even contradictory in different metal incorporated DLC films. In order to reveal the role of incorporated metal atoms, Choi et al. [25] used the first-principles calculations with a tetrahedron bond model, they pointed out that transition metals with unfilled d-orbitals, such as Mo, showed nonbonding characteristics and caused the decrease in both strength and directionality of the bonds; compared with transition metals, a noble metal with filled d-orbitals, such as Ag, showed antibonding characteristics and reduced both the strength and directionality more significantly; while light metals, such as Al, preferred a two-dimensional configuration with carbon. However, this tetrahedron bond model could not reveal the structural evolution due to incorporated metal atoms directly. Hence, the further insight of the stress reduction mechanism of metal incorporated DLC films combining with experimental characterization and theoretical calculations is still needed.

In this paper, Cu was selected as the incorporated metal element, since it was considered as a strong candidate element for reducing the

* Corresponding author.
E-mail address: aywang@nimte.ac.cn (A. Wang).
[1] These authors contributed equally to this work and should be considered as co-first authors.

http://dx.doi.org/10.1016/j.tsf.2017.09.001
0040-6090/

residual stress of DLC films and is inert with respect to carbon [20,26–29]. The structural evolution of Cu incorporated diamond-like carbon (Cu-DLC) films with Cu incorporation and the relationship between the structure and stress of Cu-DLC films were systematically investigated, moreover, theoretical calculations were also used to reveal the role of Cu atoms in the reduction of residual stress. In addition, the mechanical properties of the Cu-DLC films were also investigated in this study.

2. Experimental and computational details

2.1. Experimental details

Cu-DLC films were deposited on glass/silicon substrates by a hybrid ion beams deposition system [16] consisting of a DC magnetron sputtering with a Cu target (99.99%) and a linear anode-layer ion sources (LIS). Another 250 ± 5 μm silicon wafer was used to accurately estimate the internal stress. Before deposition, all substrates were sputter-cleaned for 20 min using Ar ion with a bias voltage of −100 V, and the Cu target was also cleaned using argon sputtering for 5 min. The base pressure was evacuated to 3×10^{-3} Pa. During film deposition, hydrocarbon gas (C_2H_2) was introduced into the LIS for carbon deposition, and Ar was supplied to the magnetron sputter for Cu sputtering. The Cu concentration was changed by the sputtering current, and the current was kept at 0.8, 1.0, 1.2, 1.5, 1.8 and 2.0 A, respectively. The C_2H_2 flux and Ar flux were kept at 15 and 65 sccm, respectively; the work pressure was kept at about 0.5 Pa. Typical values of LIS voltage and current were 1200 V and 0.2 A, respectively. A negative pulsed bias voltage of −100 V (350 kHz, 1.1 μs) was applied to the substrate. The deposition time was 15 min. For comparison, DLC film was also prepared using only LIS and a negative substrate bias of −100 V.

Surface profilometer (Alpha-Step IQ, US) was applied to measure thickness of the films, through a step between the films and bare Si wafers covered with a shadow mask. X-ray photoelectron spectroscopy (XPS, Axis ultradld, Japan) with Al (mono) Kα irradiation at pass energy 160 eV was used to characterize the chemical composition and chemical bonds of the films. Before measurement, the Ar ion beam of 3 keV was used to etch the sample surface for 5 min to remove any contaminants. X-ray diffraction (XRD, Bruker D8 Advance, Germany) with a secondary monochromator selecting the Cu Kα radiation, was used to analyze crystal structure of films deposited on glass. High-resolution transmission electron microscopy (TEM, Tecnai F20, US), operated at 200 kV with a point-to-point resolution of 0.24 nm, was used to characterize the microstructure of the deposited films. The samples for TEM were prepared by the grinding, dimpling, and ion-beam milling method. Raman spectroscopy (Renishaw inVia-reflex, UK) with a wavelength of 532 nm was used to measure the atomic bonds of the films at a detecting range from 800 to 2000 cm^{-1}, and the laser power was 6 mW.

The residual stress of the films was calculated from the curvature of film/substrate composite using the Stoney eq. [30], and a laser tester (J&L Tech Co. Ltd., JLCST022) was used to determine the curvature of film/substrate composite. Nano-indentor (MTS-G200, US) was applied to measure mechanical properties, with depth 200 nm, and the hardness was chosen in a depth of around 1/10 of the coating thickness in order to avoid the contribution of Si substrate to the results, and 6 replicate indentations were performed for each sample.

2.2. Computational details

Fig. 1 shows the employed tetrahedral bond model, in which four carbon atoms were arranged as a tetrahedron with either a carbon or Cu in the center and each peripheral carbon atom was terminated by hydrogen atoms. This model had been proved to be satisfactory to provide a reasonable explanation for the experiments in amorphous carbon system [11,25,31]. The structure with a bond angle of 109.471° in Fig. 1a was chosen as a reference state. When the bond angle was distorted in a range of 90–130° shown in Fig. 1b, the structural relaxation was

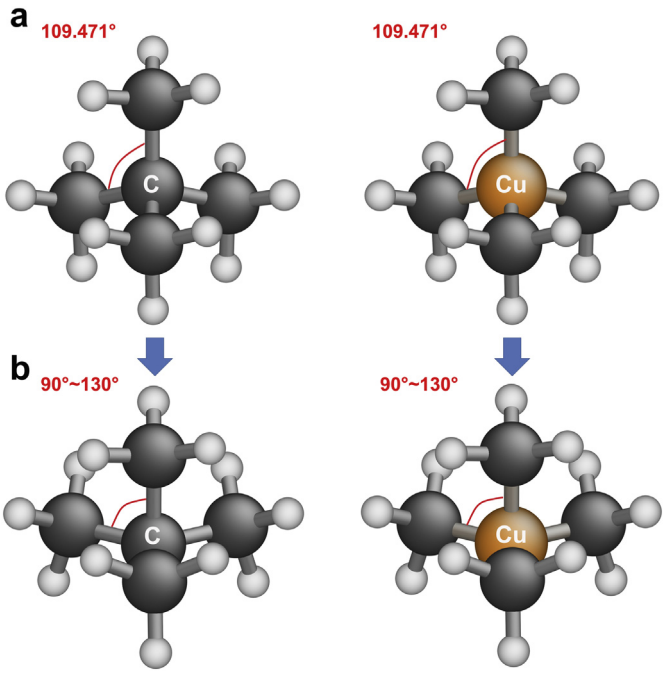

Fig. 1. Tetrahedral bond model with C or Cu atom located in the center [31]. (a) Reference state for the model with bond angles of 109.471°. (b) Distorted model with the bond angles in a range of 90–130°. The white, black and orange colors indicate the H, C and Cu atoms, respectively.

characterized from the electronic structure and the change of total energy in Cu—C system. The spin-polarized first-principles calculations based on the density functional theory were performed by the DMol^3 software package. During the calculation, the exchange-correlation was defined by the generalized gradient approximation (GGA) with the Perdew-Burke-Ernzerhof (PBE) parameterization [32] and all electrons double-numerical polarization basis set was used. The convergence criterion for structure relaxation and energy calculation with orbital cutoff of 9 Å was set with the tolerance of self-consistent field and maximum force of 10^{-5} eV and 0.01 eV/Å, respectively. A cubic supercell with a lateral size of 15 Å was used to avoid interactions between the adjacent images of the model. The electronic change caused by Cu incorporation was analyzed by the partial density of states and charge distribution of the highest occupied molecular orbital.

In order to reveal the structural evolution including the distorted bond angles and bond length, the first-principles molecular dynamics simulations were also carried out using the VASP [33,34] with GGA-PBE parameterization [32], Γ-only *k*-point sampling and cutoff energy of 500 eV. The initial configuration contained 64 atoms in a simple cubic supercell with constant volume and under periodic boundary conditions throughout the simulation. During the calculation, the initial system was first equilibrated at 8000 K for 1 ps to become completely liquid and eliminate its correlation to the initial configuration using a canonical ensemble with a Nose thermostat for temperature-control and a time step of 1 fs; then the incorporated Cu atoms were introduced into the system by substituting carbon atoms in the liquid state with an external equilibrium at 8000 K for 0.5 ps. After that, the system was quenched from 8000 to 1 K at cooling rate of 1.6×10^{16} K/s. For the subsequent geometric optimization of amorphous structure, a full relaxation of atomic positions based on conjugated gradient method [35] was repeated until the force on each atom was below 0.01 eV/Å, and the self-consistent loop was created using an energy convergence criterion of 10^{-5} eV. The computational details were referred from previous study [36]. In this calculation, Cu concentration of 1.56 at.% was selected, corresponding to 1 Cu atom in 64-atom system. DLC film was also considered for comparison. The final obtained structures of DLC and Cu-DLC films are given in Fig. 2.

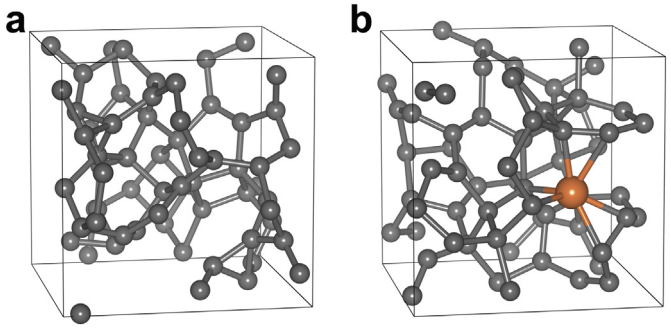

Fig. 2. Final morphologies of (a) DLC and (b) Cu-DLC film with Cu concentrations of 1.56 at.% obtained from first-principle molecular dynamics simulation. Black and orange colors indicate C and Cu atoms, respectively.

3. Results and discussion

3.1. Thickness and composition

Fig. 3 presents the average growth rates for all samples at different sputtering current. Clearly, the growth rate remarkably increased from 14 to 80 nm/min when the sputtering current increased from 0 to 2.0 A. This was due to the higher sputtering yield of Cu at higher sputtering current while keeping the constant of the hydrocarbon gas pressure [21]. Fig. 4 shows the ratio of atomic concentration of Cu in the film as a function of sputtering current. The Cu concentration was deduced based on the atomic sensitivity factors and the area ratio of C 1s to Cu 2p peaks in the XPS spectra, and the relative atomic composition ratio was considered as a sum of carbon and copper, since O concentration ranged from 0.64 to 1.68 at.% in our work and hydrogen could not be detected by XPS. It should be noted that as the sputtering current increased from 0 to 2.0 A, the Cu concentration of the films increased from 0 to 39.7 at.%.

Fig. 5a and b display the XPS C 1s spectra and Cu 2p spectra of the films with different Cu concentration, respectively. In Fig. 5a, C 1s spectra of all the films showed certain peaks, one around 284.5 eV corresponding to the sp^2-C, the other one around 285.3 eV for the sp^3-C, and C—O/C═O around 288.1 eV for some samples due to long exposure to air or possible incorporation of the oxygen during films deposition [37–39]. For Cu 2p spectra in Fig. 5b, two peaks could be well observed at around 952.7 and 932.8 eV, which corresponded to Cu (2p 1/2) and Cu (2p 3/2), respectively [22,39], implying that no carbide particles were observed.

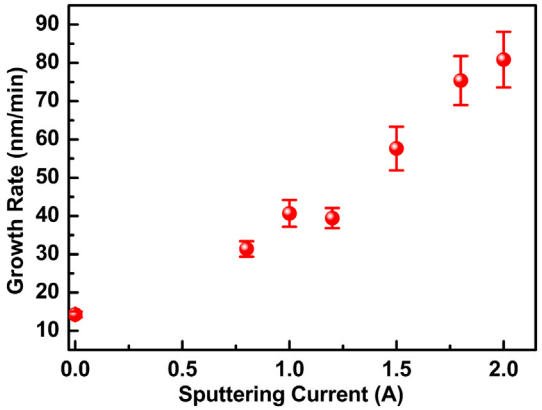

Fig. 3. Growth rates of films as a function of sputtering current.

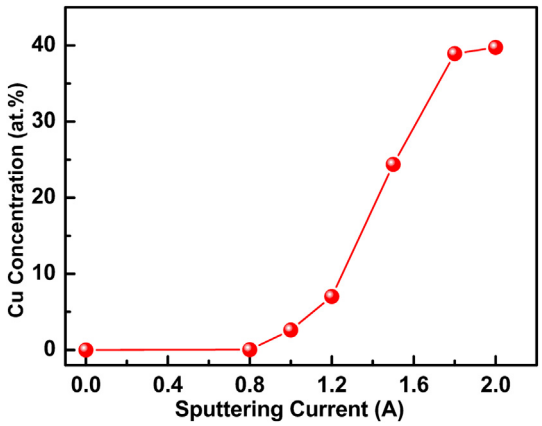

Fig. 4. Cu concentration in the films as a function of sputtering current.

3.2. XRD and TEM analysis

Fig. 6 displays the typical XRD patterns of Cu-DLC films with various Cu concentrations. When the Cu concentration was 39.7 at.%, two peaks were obtained at 43.3° and 50.4° which matched well with the face-centered cubic (FCC) copper phase and corresponded to Cu (111) and Cu (200), respectively [20]; according to Scherrer formula, the size of Cu crystallite determined from the integral width of the (111) diffraction peak was about 6 nm. As the Cu concentration was less than 39.7 at.%, the peak of Cu (200) could not be detected; the Cu (111) peak also

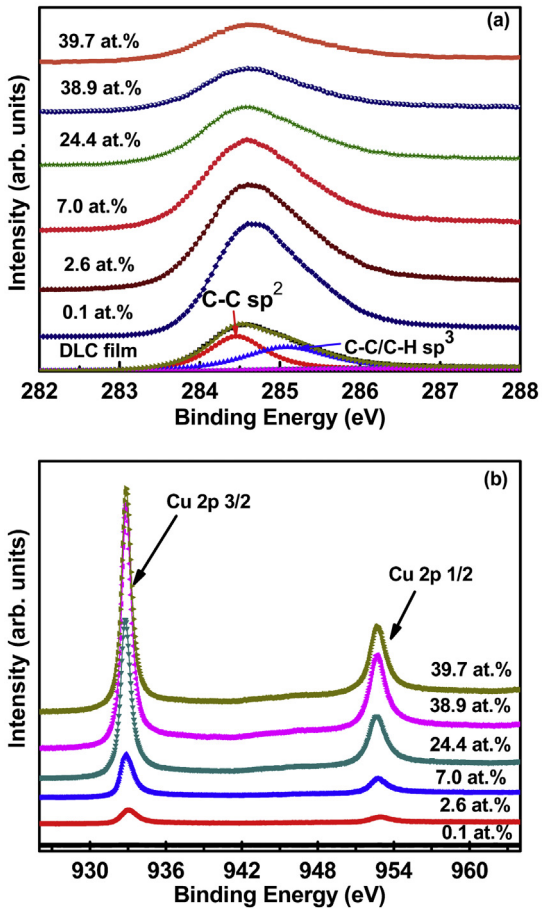

Fig. 5. (a) XPS C 1s spectra and (b) Cu 2p spectra of the films with different Cu concentrations.

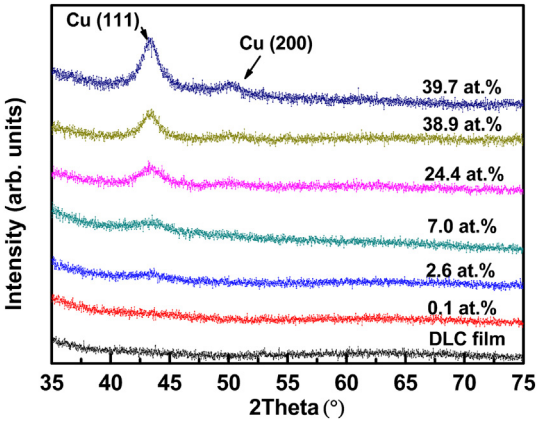

Fig. 6. XRD patterns of Cu-DLC films with various Cu concentrations.

disappeared when the Cu concentration was less than 7.0 at.%. It implied that nanoscale Cu particles existed in the DLC matrix when Cu concentration was larger than 7.0 at.%.

In order to further investigate the structural evolution of the Cu-DLC films, high resolution transmission electron microscopy (HRTEM) and corresponding selected area electron diffraction (SAED) were used. As shown in Fig. 7a, when the Cu concentration was 2.6 at.%, there was no crystalline phase existed in the plan-view image, and the corresponding SAED only showed a diffused ring, which indicated a homogeneous and amorphous structure, similar to that of pure DLC [16]. However, some sharp crystalline diffraction rings were observed as the Cu concentration increased to 7.0 at.% (Fig. 7b), indicating the existence of polycrystalline phases, which were identified to be the (111), (200), (220), (311) and (420) reflections of the FCC Cu phase. Compared with the XRD patterns, it could be concluded that the Cu crystalline phase began to evolve in the DLC matrix when Cu concentration was in the range of 2.6–7.0 at.%.

3.3. Raman analysis

Fig. 8a displays the Raman spectra of the films as a function of Cu concentration. According to the XRD result, the FCC Cu crystalline phase is centrosymmetric, so Raman spectra are obtained from the carbon matrix only. Obviously, all samples presented a broad asymmetric Raman scattering band in the range of 1000–1700 cm^{-1}. Two Gaussian peaks, G-peak (graphite) at around 1580 cm^{-1} corresponding to E_{2g} symmetry stretching vibration mode and shoulder D-peak (disorder) at around 1360 cm^{-1} corresponding to the zone edge of A_{1g} breathing mode, were used to fit the experimental spectra after background correction [1]. The bond disorder, sp^2/sp^3 ratio, sp^2 site clustering of the films can be derived qualitatively according to the fitted G-peak position, the peak area ratio of D-peak to G-peak (I_D/I_G), the full width at half maximum of G-peak (G_{FWHM}) [40,41]. As shown in Fig. 8b, with Cu concentration increasing, the G peak position shifted upwards from 1540 cm^{-1} for pure carbon film to 1557 cm^{-1} and the I_D/I_G ratio also increased from 0.8 to 2.4, implying the increase of sp^2/sp^3 ratio and C-sp^2 cluster size. Also, Fig. 8c showed that G_{FWHM} decreased from 192 cm^{-1} to 127 cm^{-1} with the increase of Cu concentration, suggesting that the degree of film structural disorder declined.

3.4. Stress analysis

Fig. 9 presents the residual stress of the films as a function of Cu concentration. Compared with the high stress of DLC film (2.0 GPa), a significant reduction of residual stress was observed for all the Cu-DLC films. When the Cu concentration increased from 0 to 2.6 at.%, the residual stress decreased remarkably from 2.0 to 0.032 GPa, then increased to 0.56 GPa at 24.4 at.%, after that the residual stress decreased slightly to 0.40 GPa at 39.7 at.%. Similar results can be referred in [10,11,20]. Taking into account the microstructure, it was safe to conclude that the residual stress was closed related to the structural evolution. When Cu concentration was less than 2.6 at.%, the metal atoms were dissolved in the DLC matrix, which could reduce the strain energy arising from the distortion of the atomic bond structure, resulting in a significant reduction of the residual stress; as Cu concentration exceeded 7.0 at.%, nanoscale Cu particles were distributed uniformly in the DLC matrix, then Cu-DLC films could still maintain a low-level stress, which was similar in Al [15], Ag [17,18] and Au-incorporated [19] DLC films, but remarkably different from the Mo [13], W [10], Ti [14] and Cr-incorporated [16] DLC films. This can be explained from the fact that nanoscale Cu/Al/Ag/Au particles were much softer compared with WC_{1-x}, CrC, TiC and MoC phases, so deformation caused by highly distorted DLC matrix in those soft nanoscale metal particles can occur, which resulted in less structural disorder compared with DLC films and residual stress reduction. While, in the range of 2.6–7.0 at.%, the residual stress also depended on the change of the atomic bond structure as dissolved Cu atoms began to form nanoscale Cu particles.

In order to gain insight into the experimental results and reveal the stress reduction mechanism, the electronic and atomic bond structure of Cu-DLC films were also investigated [42]. Firstly, the bond characteristics between Cu and C atom were studied by first-principles

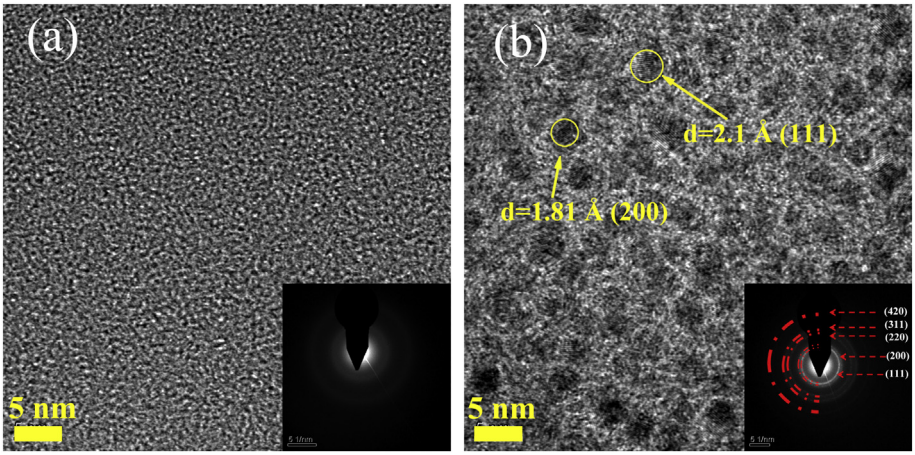

Fig. 7. Plan-view HRTEM and corresponding SAED patterns of Cu-DLC films with (a) 2.6 at.% and (b) 7.0 at.% Cu atoms.

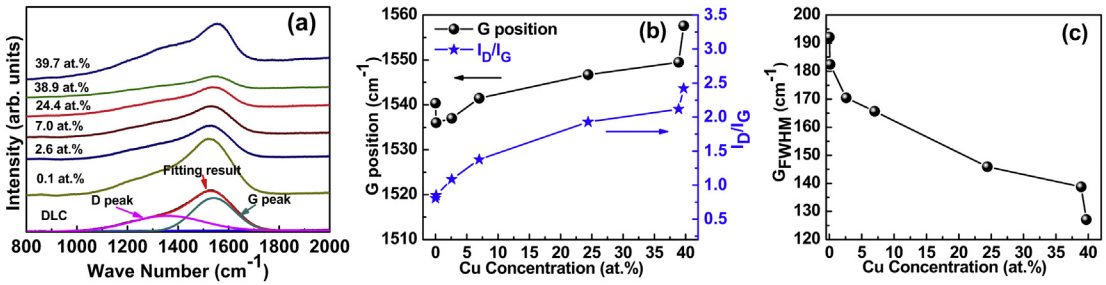

Fig. 8. (a) Raman spectra, (b) G peak position and I_D/I_G, and (c) G_{FWHM} of the films with different Cu concentrations.

calculation based on density functional theory (DFT) using the simplified tetrahedral structure model [25]. Fig. 10a presents the energy change via bond angle distortion in Cu—C and the pure C—C system. It showed that with the bond angle distortion, the energy change was decreased seriously comparing with C—C system. Because the residual stress was closely related with the distortion energy, the addition of Cu atoms into amorphous carbon matrix would decrease the residual stress due to the lowered distortion energy. In order to clarify the energy change, the bond characteristics were analyzed by the analysis of partial density of states (PDOS) and charge distribution of the highest occupied molecular orbital (HOMO), as shown in Fig. 10b. According to molecular orbital theory, the HOMO of Cu—C was antibonding, which reduced the strength of bond and stability of system. So it led to the small distortion energy change. The simulation was largely in accordance with our experimental results.

It is known that the residual stress in DLC films was closely related with the distorted bond structure. So the first-principles molecular dynamics simulation was undertaken to provide the change of atomic bond structure including both the bond angles and bond length distributions in Cu-DLC films as shown in Fig. 11. The equilibrium bond angle of graphite is 120° and the diamond one is 109.471° (Fig. 11a); the equilibrium bond length of graphite is 1.42 Å and the diamond one is 1.54 Å (Fig. 11b). Previous study has revealed that the high compressive stress mainly originated from the distortion of bond angles and bond lengths, which were less than 109.471° and 1.42 Å, respectively [43]. It can be found that when the Cu concentration increased from 0 to 1.56 at.%, the population of bond length smaller than 1.42 Å and the bond angle smaller than 109.471° decreased simultaneously comparing with DLC film, which implied that the incorporation of Cu into DLC films affected the distorted structure of carbon matrix, and led to the significant reduction of compressive stress. Therefore, the stress reduction mechanism caused by Cu attributed to the weak Cu—C bond and the decreased fraction of distorted structures.

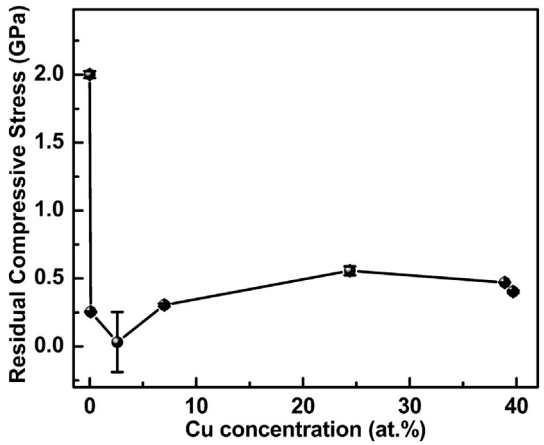

Fig. 9. Residual stress of Cu-DLC films as a function of Cu concentration.

3.5. Hardness analysis

Fig. 12 depicts the hardness and elastic modulus as a function of Cu concentration. It clearly showed that as the Cu concentration increased from 0 to 39.7 at.%, the hardness and elastic modulus of the films decreased obviously from 25.3 to 4.97 GPa, 216 to 90.7 GPa, respectively. According to its structural evolution, at least three key factors should be considered. First, the incorporation of Cu atoms caused a higher sp^2/sp^3 ratio, while the mechanical properties of DLC films mainly depended on its sp^3 carbon matrix [1]; moreover, the nanoscale Cu particles present at higher Cu concentration would break up the continuity of the carbon network; besides, the increase of soft Cu content could also influence the harness of the composite films, resulting in a reduction of both hardness and elastic modulus of the films.

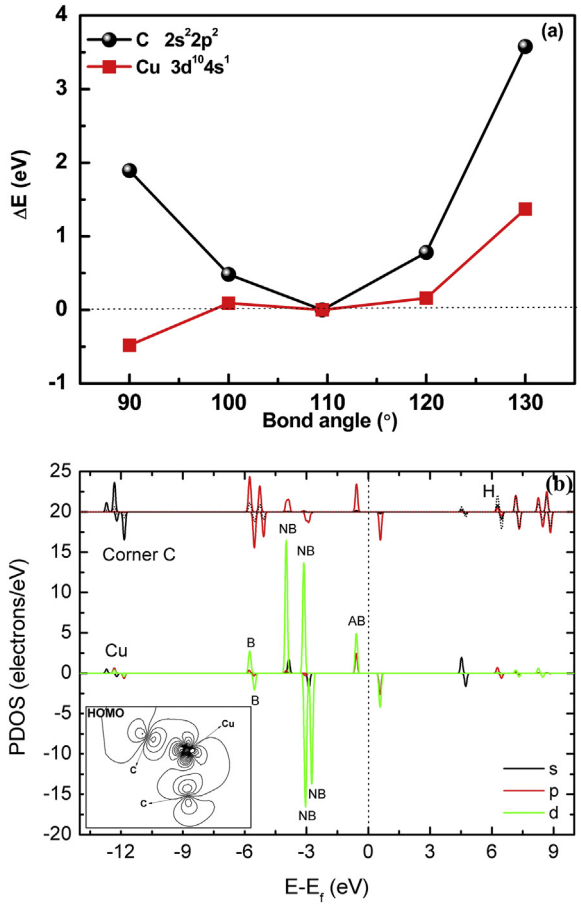

Fig. 10. First-principle calculation results [31]: (a) energy change via bond angle distortion in Cu—C and the pure C—C system; (b) PDOS projected on the central Cu and corner C atoms in the Cu—C system, in which the inset shows the charge density between the central Cu or C and corner C atoms for the HOMO passing through Cu and two corner C atoms.

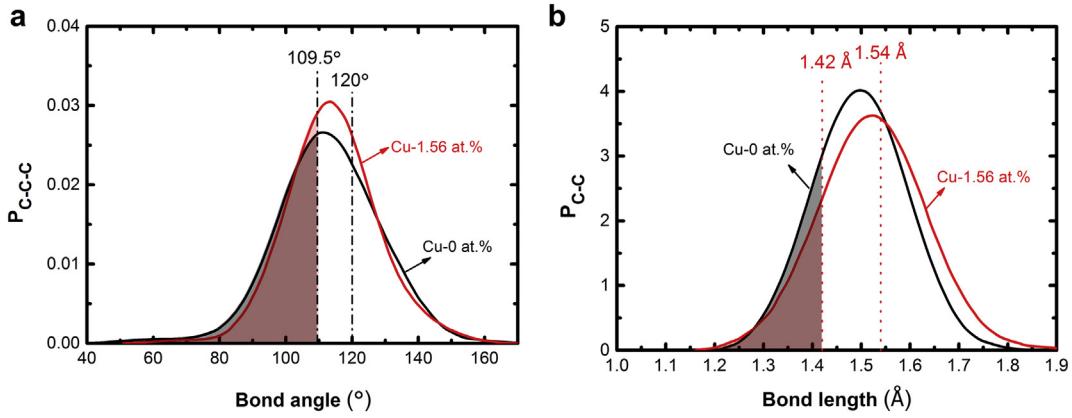

Fig. 11. (a) bond angles distribution functions (b) bond lengths distribution functions of Cu-DLC films with Cu concentration of 0 and 1.56 at.%, respectively.

4. Conclusions

The Cu-DLC films with Cu concentration varying from 0.1 to 39.7 at.% were prepared on the silicon/glass substrates by a hybrid beams deposition system with Cu target (99.99%) and C_2H_2 precursor gas. Compositional and structural analysis showed that nanoscale Cu particles began to evolve from the carbon matrix in the range of 2.6–7.0 at.%, and the incorporation of Cu would result in a higher sp^2/sp^3 ratio and bigger C-sp^2 cluster. The residual stresses of the Cu-DLC films ranged from 0.032 to 0.56 GPa, showing a significant decrease compared with that of the DLC film, which could be due to metal atoms distribution and deformation in nanoscale Cu particles in different Cu concentration range. Theoretical calculation based on DFT revealed that the addition of Cu atoms into amorphous carbon matrix would decrease the residual stress due to formation of Cu—C antibonding and the relaxation of distorted bond angles and bond length.

Acknowledgements

The present research was financially supported by National Natural Science Foundation of China (51522106, 51772307, 51602319), Korea Research Fellowship Program through the National Research Foundation of Korea (NRF) funded by the Ministry of Science and ICT (2017H1D3A1A01055070). The authors thank Prof. Liang Chen at Ningbo Institute of Materials Technology and Engineering, Chinese Academy of Sciences, for providing the supercomputer platform and productive discussion.

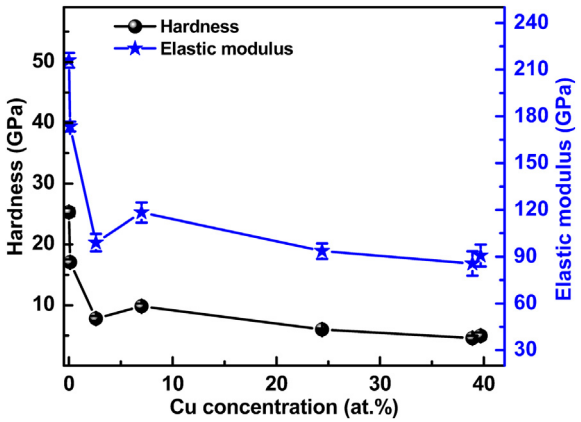

Fig. 12. Hardness and elastic modulus of Cu-DLC films as a function of Cu concentration.

References

[1] J. Robertson, Diamond-like amorphous carbon, Mater. Sci. Eng. B 37 (2002) 129–281.
[2] N. Dwivedi, S. Kumar, J.D. Carey, R.K. Tripathi, H.K. Malik, M.K. Dalai, Influence of silver incorporation on the structural and electrical properties of diamond-like carbon thin films, ACS Appl. Mater. Interfaces 5 (2013) 2725–2732.
[3] G.A. Abbas, S.S. Roy, P. Papakonstantinou, J.A. McLaughlin, Structural investigation and gas barrier performance of diamond-like carbon based films on polymer substrates, Carbon 43 (2005) 303–309.
[4] D. Banerjee, S. Mukherjee, K.K. Chattopadhyay, Controlling the surface topology and hence the hydrophobicity of amorphous carbon thin films, Carbon 48 (2010) 1025–1031.
[5] A. Yan, X. Xiao, I. Külaots, B.W. Sheldon, R.H. Hurt, Controlling water contact angle on carbon surfaces from 5° to 167°, Carbon 44 (2006) 3116–3120.
[6] C.P.O. Treutler, Industrial use of plasma-deposited coatings for components of automotive fuel injection systems, Surf. Coat. Technol. 200 (2005) 1969–1975.
[7] B. Zheng, W.T. Zheng, S.S. Yu, H.W. Tian, F.L. Meng, Y.M. Wang, J.Q. Zhu, S.H. Meng, X.D. He, J.C. Han, Growth of tetrahedral amorphous carbon film: tight-binding molecular dynamics study, Carbon 43 (2005) 1976–1983.
[8] M. Lejeune, M. Benlahsen, R. Bouzerar, Stress and structural relaxation in amorphous hydrogenated carbon films, Appl. Phys. Lett. 84 (2004) 344.
[9] C. Corbella, M. Vives, A. Pinyol, E. Bertran, C. Canal, M.C. Polo, J.L. Andújar, Preparation of metal (W, Mo, Nb, Ti) containing a-C:H films by reactive magnetron sputtering, Surf. Coat. Technol. 177-178 (2004) 409–414.
[10] A.Y. Wang, H.S. Ahn, K.R. Lee, J.P. Ahn, Unusual stress behavior in W-incorporated hydrogenated amorphous carbon films, Appl. Phys. Lett. 86 (2005) 111902.
[11] A.Y. Wang, K.R. Lee, J.P. Ahn, J.H. Han, Structure and mechanical properties of W incorporated diamond-like carbon films prepared by a hybrid ion beam deposition technique, Carbon 44 (2006) 1826–1832.
[12] P. Guo, P.L. Ke, A.Y. Wang, Incorporated W roles on microstructure and properties of W-C:H films by a hybrid linear ion beam systems, J. Nanomater. 2013 (2013) 1–8.
[13] L. Ji, H. Li, F. Zhao, J. Chen, H. Zhou, Microstructure and mechanical properties of Mo/DLC nanocomposite films, Diam. Relat. Mater. 17 (2008) 1949–1954.
[14] W. Dai, P. Ke, M.-W. Moon, K.-R. Lee, A. Wang, Investigation of the microstructure, mechanical properties and tribological behaviors of Ti-containing diamond-like carbon films fabricated by a hybrid ion beam method, Thin Solid Films 520 (2012) 6057–6063.
[15] B.K. Tay, Y.H. Cheng, X.Z. Ding, S.P. Lau, X. Shi, G.F. You, D. Sheeja, Hard carbon nanocomposite films with low stress, Diam. Relat. Mater. 10 (2001) 1082–1087.
[16] W. Dai, G.S. Wu, A.Y. Wang, Preparation, characterization and properties of Cr-incorporated DLC films on magnesium alloy, Diam. Relat. Mater. 19 (2010) 1307–1315.
[17] H.W. Choi, J.H. Choi, K.R. Lee, J.P. Ahn, K.H. Oh, Structure and mechanical properties of Ag-incorporated DLC films prepared by a hybrid ion beam deposition system, Thin Solid Films 516 (2007) 248–251.
[18] Y. Wu, J. Chen, H. Li, L. Ji, Y. Ye, H. Zhou, Preparation and properties of Ag/DLC nanocomposite films fabricated by unbalanced magnetron sputtering, Appl. Surf. Sci. 284 (2013) 165–170.
[19] R. Paul, S.R. Bhattacharyya, R. Bhar, A.K. Pal, Modulation of residual stress in diamond like carbon films with incorporation of nanocrystalline gold, Appl. Surf. Sci. 257 (2011) 10451–10458.
[20] C.C. Chen, F.C.N. Hong, Structure and properties of diamond-like carbon nanocomposite films containing copper nanoparticles, Appl. Surf. Sci. 242 (2005) 261–269.
[21] J. Musil, M. Louda, Z. Soukup, M. Kubásek, Relationship between mechanical properties and coefficient of friction of sputtered a-C/Cu composite thin films, Diam. Relat. Mater. 17 (2008) 1905–1911.
[22] L.N. Huang, H.Q. Jiang, J.S. Zhang, Z.J. Zhang, P.Y. Zhang, Synthesis of copper nanoparticles containing diamond-like carbon films by electrochemical method, Electrochem. Commun. 8 (2006) 262–266.
[23] Q. Wang, F. Zhou, Z. Zhou, Y. Yang, C. Yan, C. Wang, W. Zhang, L.K.Y. Li, I. Bello, S.T. Lee, Influence of Ti content on the structure and tribological properties of Ti-DLC coatings in water lubrication, Diam. Relat. Mater. 25 (2012) 163–175.

[24] Q. Wang, F. Zhou, X. Ding, Z. Zhou, C. Wang, W. Zhang, L.K.Y. Li, S.T. Lee, Structure and water-lubricated tribological properties of Cr/a-C coatings with different Cr contents, Tribol. Int. 67 (2013) 104–115.
[25] J.H. Choi, S.C. Lee, K.R. Lee, A first-principles study on the bond characteristics in carbon containing Mo, Ag, or Al impurity atoms, Carbon 46 (2008) 185–188.
[26] A. Pardo, J.G. Buijnsters, J.L. Endrino, C. Gómez-Aleixandre, G. Abrasonis, R. Bonet, J. Caro, Effect of the metal concentration on the structural, mechanical and tribological properties of self-organized a-C:Cu hard nanocomposite coatings, Appl. Surf. Sci. 280 (2013) 791–798.
[27] A. Jurkevičiūtė, A. Lazauskas, T. Tamulevičius, A. Vasiliauskas, D. Peckus, Š. Meškinis, S. Tamulevičius, Structure and density profile of diamond-like carbon films containing copper: study by X-ray reflectivity, transmission electron microscopy, and spectroscopic ellipsometry, Thin Solid Films 630 (2017) 48–58.
[28] A.S. Chaus, T.N. Fedosenko, A.V. Rogachev, Ľ. Čaplovič, Surface, microstructure and optical properties of copper-doped diamond-like carbon coating deposited in pulsed cathodic arc plasma, Diam. Relat. Mater. 42 (2014) 64–70.
[29] Š. Meškinis, A. Čiegis, A. Vasiliauskas, K. Šlapikas, T. Tamulevičius, A. Tamulevičienė, S. Tamulevičius, Optical properties of diamond like carbon films containing copper, grown by high power pulsed magnetron sputtering and direct current magnetron sputtering: structure and composition effects, Thin Solid Films 581 (2015) 48–53.
[30] G.G. Stoney, The tension of metallic films deposited by electrolysis, Proc. R. Soc. London, Ser. A 82 (1909) 172–175 (Containing papers of a mathematical and physical character).
[31] X.W. Li, D. Zhang, K.R. Lee, A.Y. Wang, Effect of metal doping on structural characteristics of amorphous carbon system: a first-principles study, Thin Solid Films 607 (2016) 67–72.
[32] J.P. Perdew, K. Burke, M. Ernzerhof, Generalized gradient approximation made simple, Phys. Rev. Lett. 77 (1996) 3865–3868.
[33] G. Kresse, J. Furthmülle, Efficiency of ab-initio total energy calculations for metals and semiconductors using a plane-wave basis set, Comput. Mater. Sci. 6 (1996) 15–50.
[34] G. Kresse, J. Furthmülle, Efficient iterative schemes for ab initio total-energy calculations using a plane-wave basis set, Phys. Rev. B 54 (1996) 11169–11186.
[35] M.J. Gillan, Calculation of the vacancy formation energy in aluminium, J. Phys. Condens. Matter 1 (1989) 689–711.
[36] X.W. Li, P.L. Ke, A.Y. Wang, Probing the stress reduction mechanism of diamond-like carbon films by incorporating Ti, Cr, or W carbide-forming metals: ab initio molecular dynamics simulation, J. Phys. Chem. C 119 (2015) 6086–6093.
[37] D. Bourgoin, S. Turgeon, G.G. Ross, Characterization of hydrogenated amorphous carbon films produced by plasma-enhanced chemical vapour deposition with various chemical hybridizations, Thin Solid Films 357 (1999) 246–253.
[38] Y. Taki, O. Takai, XPS structural characterization of hydrogenated amorphous carbon thin films prepared by shielded arc ion plating, Thin Solid Films 316 (1998) 45–50.
[39] Y.M. Foong, A.T.T. Koh, S.R. Lim, D.H.C. Chua, H.Y. Ng, Properties of laser fabricated nanostructured Cu/diamond-like carbon composite, J. Mater. Res. 26 (2011) 2761–2771.
[40] A.C. Ferrari, J. Robertson, Interpretation of Raman spectra of disordered and amorphous carbon, Phys. Rev. B 61 (2000) 14095–14107.
[41] C. Casiraghi, A.C. Ferrari, J. Robertson, Raman spectroscopy of hydrogenated amorphous carbons, Phys. Rev. B 72 (2005), 085401.
[42] X.W. Li, K.R. Lee, A.Y. Wang, Chemical bond structure of metal-incorporated carbon system, J. Comput. Theor. Nanosci. 10 (2013) 1688–1692.
[43] X.W. Li, P.L. Ke, H. Zheng, A.Y. Wang, Structural properties and growth evolution of diamond-like carbon films with different incident energies: a molecular dynamics study, Appl. Surf. Sci. 273 (2013) 670–675.